Frontiers of Information Technology & Electronic Engineering
www.jzus.zju.edu.cn; engineering.cae.cn; www.springerlink.com
ISSN 2095-9184 (print); ISSN 2095-9230 (online)
E-mail: jzus@zju.edu.cn

Mutual-information based weighted fusion for target tracking in underwater wireless sensor networks*

Duo ZHANG[1,2], Mei-qin LIU‡[1,2], Sen-lin ZHANG[2], Zhen FAN[2], Qun-fei ZHANG[3]

[1]*State Key Laboratory of Industrial Control Technology, Zhejiang University, Hangzhou 310027, China*

[2]*College of Electrical Engineering, Zhejiang University, Hangzhou 310027, China*

[3]*School of Marine Science and Technology, Northwestern Polytechnical University, Xi'an 710072, China*

E-mail: {zhangduo, liumeiqin, slzhang, fanzhen}@zju.edu.cn; zhangqf@nwpu.edu.cn

Received Nov. 9, 2016; Revision accepted Mar. 14, 2017; Crosschecked Apr. 3, 2018

Abstract: Underwater wireless sensor networks (UWSNs) can provide a promising solution to underwater target tracking. Due to limited energy and bandwidth resources, only a small number of nodes are selected to track a target at each interval. Because all measurements are fused together to provide information in a fusion center, fusion weights of all selected nodes may affect the performance of target tracking. As far as we know, almost all existing tracking schemes neglect this problem. We study a weighted fusion scheme for target tracking in UWSNs. First, because the mutual information (MI) between a node's measurement and the target state can quantify target information provided by the node, it is calculated to determine proper fusion weights. Second, we design a novel multi-sensor weighted particle filter (MSWPF) using fusion weights determined by MI. Third, we present a local node selection scheme based on posterior Cramer-Rao lower bound (PCRLB) to improve tracking efficiency. Finally, simulation results are presented to verify the performance improvement of our scheme with proper fusion weights.

Key words: Target tacking; Fusion weight; Mutual information; Node selection; Underwater wireless sensor networks

https://doi.org/10.1631/FITEE.1601695 **CLC number:** TN92

1 Introduction

Today, underwater target tracking is an increasingly important issue in many civilian and military fields, such as modern underwater military defense systems, underwater vehicle navigation and control, and intelligent traffic management systems. Because of the importance of underwater target tracking, many underwater target tracking algorithms with sonar array have been proposed (Pettersson et al., 2005; Asif et al., 2006; Dalberg et al., 2006; Georgy et al., 2012). Because sonar arrays need to be pulled by a ship or submarine, these algorithms are not adaptive to harsh underwater environments. Once the ship or submarine is under attack, the entire tracking system will fail.

Different from sonar arrays, underwater wireless sensor networks (UWSNs) provide a more reliable solution to underwater target tracking. UWSNs are inexpensive, small, and self-organized, can be deployed in a widespread area, and can therefore offer a more reliable, precise, concealed, and persistent tracking solution (Pettersson et al., 2005; Asif et al., 2006; Dalberg et al., 2006; Georgy et al., 2012). Consequently, research has been carried out, and results have been reported concerning target tracking in UWSNs. Instead of a complete tracking algorithm, Zhou and Willett (2007) designed only the

‡ Corresponding author

* Project supported by the National Natural Science Foundation of China (Nos. 61531015, 61673345, and 61374021) and the NSFC-Zhejiang Joint Fund for the Integration of Industrialization and Informatization (Nos. U1609204 and U1709203)

ORCID: Mei-qin LIU, http://orcid.org/0000-0003-0693-6574

location estimation algorithm. To know the size of an underwater target, Liang and Cheng (2009) proposed an estimation algorithm based on maximum likelihood, but an entire tracking solution is still not available. Huang et al. (2008) presented two tracking algorithms that are based on a distributed particle filter (PF) for cluster-based underwater sensor networks, one of which provides a more precise tracking result, while the other focuses on dramatic reduction of energy consumption and tracking efficiency. Wang et al. (2012) combined PF with an interactive multiple model to solve nonlinear and maneuvering target tracking problems in three dimensions, but they did not consider the energy consumption problem, and thus their algorithm is not practical for UWSNs. Isbitiren and Akan (2011) presented a target tracking algorithm in three-dimensional UWSNs. First, the distance from a node to its target was calculated with the echo time of arrival (TOA) from the target after transmitting acoustic pulses from the sensors, and the trilateration method was used to obtain the target's location. Then the location and calculated velocity of the target were exploited to achieve tracking. As we know, energy consumption is also a critical issue for target tracking in UWSNs. To extend the lifetime of the system, Yu et al. (2008) used a wake-up/sleep scheme to select a number of nodes to track the underwater target at each sampling interval. However, the target-node geometry and fusion weights of selected nodes were not considered. Baumgartner et al. (2009a) derived an integral objective function representing the quality of the service of a sensor network performing cooperative tracking detection over time using a geometric transversal approach. Then optimal control was used for cooperative target tracking in UWSNs. To improve the service quality of a sensor network for cooperative tracking detection, Baumgartner et al. (2009b) proposed a novel approach comprising placing sensors in the region of interest based on their future displacement.

To the best of our knowledge, target-node geometry affects the accuracy of target tracking in UWSNs, and our previous study provided some solutions to select the optimal target-node geometry for target tracking (Zhang Q et al., 2014, 2015; Liu et al., 2016; Zhang et al., 2016). The relationship between the posterior Cramer-Rao lower bound (PCRLB) and the target-node geometry was derived, and a node selection scheme was designed by minimizing the PCRLB. As we know, the information from different nodes varies due to node differences such as position and distance to the target (Chen et al., 2010; Javadi and Peiravi, 2015), but the fusion weights of selected nodes are equal; it is not a precise approach for practical tracking tasks. Therefore, it is important to consider the fusion weights of selected nodes for tracking. To overcome this limitation, we study fusion weights of selected nodes and present a novel scheme to design fusion weights. This scheme has more precise tracking results than our previous study. The main contributions of this paper can be summarized as follows:

1. We derive the mutual information (MI) between a node's measurement and the target state in an underwater environment. It considers the effect of the node's location uncertainty due to mobility.

2. We propose a novel scheme to design fusion weights by using MI, which can quantify information about the target by the node's measurement.

3. We present a novel multi-sensor weighted particle filter (MSWPF). Combined with a node selection scheme based on the PCRLB, we offer a more precise and energy-efficient target-tracking solution to UWSNs.

2 Problem formulation

In this section, we formulate the problem of single target tracking in UWSNs. The relevant issues include the network model, the target state model, and the measurement model.

2.1 Network model

As an example (Fig. 1), sensor nodes in UWSNs are anchored to the ocean bottom to perform the target tracking task. Sensor nodes are deployed at known positions along the ocean floor. Different from terrestrial sensor networks, underwater nodes move due to the effect of water flow. Therefore, the true locations of the nodes are not fixed; we know only the estimated locations of nodes. If a moving target is within the sensing range of a node, the node will wake up, participate in the tracking task, measure the target, and send quantized measurements to the fusion center. Otherwise, it remains dormant for energy efficiency. After receiving measurements from all selected nodes, the fusion center will estimate the

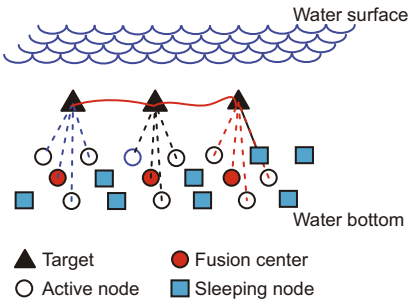

Fig. 1 Network model

target state via a tracking algorithm.

2.2 Target state model

We assume the target to be a slowly maneuvering point that moves at a known depth. For simplicity, the nearly constant velocity (CV) model can be used. Note that our scheme is not limited to the CV model; for some complex motion models, the interacting multiple model (IMM) approach can be combined with our scheme. Thus, the target state is given by

$$\boldsymbol{x}_{k+1} = \boldsymbol{F}_k \boldsymbol{x}_k + \boldsymbol{w}_k, \tag{1}$$

where the target state at time k is given by $\boldsymbol{x}_k = [x, v_x, y, v_y]^{\mathrm{T}}$, (x, y) is the target's location, v_x and v_y are the corresponding velocities in x and y coordinates, $\boldsymbol{F}_k$ is the state transition matrix, and the process noise $\boldsymbol{w}_k$ is always assumed to be Gaussian with zero mean and covariance matrix $\boldsymbol{Q}_k$. The state transition matrix $\boldsymbol{F}_k$ and process noise covariance matrix $\boldsymbol{Q}_k$ are given as follows:

$$\boldsymbol{F}_k = \begin{bmatrix} 1 & T & 0 & 0 \\ 0 & 1 & 0 & 0 \\ 0 & 0 & 1 & T \\ 0 & 0 & 0 & 1 \end{bmatrix}, \tag{2}$$

$$\boldsymbol{Q}_k = q^2 \begin{bmatrix} \frac{T^3}{3} & \frac{T^2}{2} & 0 & 0 \\ \frac{T^2}{2} & T & 0 & 0 \\ 0 & 0 & \frac{T^3}{3} & \frac{T^2}{2} \\ 0 & 0 & \frac{T^2}{2} & T \end{bmatrix}, \tag{3}$$

where T is the sampling interval and q is the process parameter.

2.3 Measurement model

We assume that each sensor node is equipped with an acoustic sensor. The measurement model for the acoustic sensor contains the base frequency measurement model (narrow-band processing), the acoustic spectrum pattern model (narrow-band processing), and the acoustic sound pressure measurement model (wide-band processing) (Doug et al., 2002; Huang et al., 2008). Due to the effect of water flow, it is hard to know the true locations of nodes. Thus, we adopt the measurement model which considers the uncertainty of a node's location (Punithakumar et al., 2006). Assume that nodes move with water flow according to

$$\begin{cases} x^s_{k+1} = \hat{x}^s_{k+1} + \Delta x^s_{k+1}, \\ y^s_{k+1} = \hat{y}^s_{k+1} + \Delta y^s_{k+1}, \end{cases} \tag{4}$$

where (x^s_{k+1}, y^s_{k+1}) is the node's true location, $(\hat{x}^s_{k+1}, \hat{y}^s_{k+1})$ is the estimated location computed by localization algorithms (Han et al., 2012; Zhang et al., 2013; Zhang S et al., 2014), and Δx^s_{k+1} and Δy^s_{k+1} are mutually independent zero mean Gaussian white noise sequences with variances r_x^2 and r_y^2, respectively. Through the first-order Taylor series expansion around the node's estimated location, the measurement of the s^{th} sensor node at time $k+1$ is

$$\begin{aligned} m^s_{k+1,r} &= h^s_{k+1}(\boldsymbol{x}_{k+1}, x^s_{k+1}, y^s_{k+1}) + v^s_{k+1} \\ &\approx h^s_{k+1}(\boldsymbol{x}_{k+1}, \hat{x}^s_{k+1}, \hat{y}^s_{k+1}) + v^s_{k+1} \\ &\quad + \frac{\partial h^s_{k+1}}{\partial x^s_{k+1}} \Delta x^s_{k+1} + \frac{\partial h^s_{k+1}}{\partial y^s_{k+1}} \Delta y^s_{k+1} \\ &= h^s_{k+1}(\boldsymbol{x}_{k+1}, \hat{x}^s_{k+1}, \hat{y}^s_{k+1}) + \bar{v}^s_{k+1}, \end{aligned} \tag{5}$$

$$h^s_{k+1} = \frac{S}{(x^1_{k+1} - x^s_{k+1})^2 + (x^3_{k+1} - y^s_{k+1})^2 + h^2}, \tag{6}$$

$$\bar{v}^s_{k+1} = v^s_{k+1} + \frac{\partial h^s_{k+1}}{\partial x^s_{k+1}} \Delta x^s_{k+1} + \frac{\partial h^s_{k+1}}{\partial y^s_{k+1}} \Delta y^s_{k+1}, \tag{7}$$

where S is the target's source-level sound pressure, which is assumed to be constant, x^1_{k+1} and x^3_{k+1} are the first and third elements of target state vector $\boldsymbol{x}_{k+1}$, which represents the position of the target at time $k+1$, $h^s_{k+1}(\boldsymbol{x}_{k+1}, x^s_{k+1}, y^s_{k+1})$ is the received sound pressure at the s^{th} sensor node without measurement noise, v^s_{k+1} is the raw measurement noise, which is assumed to be independent across time steps and across sensors, and follows a Gaussian distribution with parameters $\mathcal{N}(0, r^2)$, and $\bar{v}^s_{k+1}$ is the equivalent measurement noise with mean and variance:

$$\begin{aligned} &E[\bar{v}^s_{k+1}] \\ &= E[v^s_{k+1}] + \frac{\partial h^s_{k+1}}{\partial x^s_{k+1}} E[\Delta x^s_{k+1}] + \frac{\partial h^s_{k+1}}{\partial y^s_{k+1}} E[\Delta y^s_{k+1}] \\ &= 0, \end{aligned} \tag{8}$$

$$
\begin{aligned}
&E[(\bar{v}^s_{k+1})^2]\\
&=E[(v^s_{k+1})^2]+\left(\frac{\partial h^s_{k+1}}{\partial x^s_{k+1}}\right)^2 E[(\Delta x^s_{k+1})^2]\\
&\quad+\left(\frac{\partial h^s_{k+1}}{\partial y^s_{k+1}}\right)^2 E[(\Delta y^s_{k+1})^2]+C\\
&=r^2+\left(\frac{\partial h^s_{k+1}}{\partial x^s_{k+1}}\right)^2 r_x^2+\left(\frac{\partial h^s_{k+1}}{\partial y^s_{k+1}}\right)^2 r_y^2+C. \qquad (9)
\end{aligned}
$$

Because three noises v^s_{k+1}, Δx^s_{k+1}, and Δy^s_{k+1} are zero mean and independent of each other, the crossing term C equals 0. Thus, the variance r_m^2 of $\bar{v}^s_{k+1}$ is obtained as

$$
r_m^2=r^2+\left(\frac{\partial h^s_{k+1}}{\partial x^s_{k+1}}\right)^2 r_x^2+\left(\frac{\partial h^s_{k+1}}{\partial y^s_{k+1}}\right)^2 r_y^2. \qquad (10)
$$

Due to the energy limitation of UWSNs, we consider the practical scenario for communication between sensor nodes and the fusion center: each node locally quantizes its raw measurement to L bits, and then transmits the quantized measurement to the fusion center for follow-up processing (Ruan et al., 2003; Duan et al., 2008; Ozdemir et al., 2009; Masazade et al., 2012). Though quantization may lose some information about the target, it alleviates the communication and computation burden.

The quantized measurement model of sensor node s at time $k+1$ is defined as

$$
m^s_{k+1,q}=\begin{cases}0, & \gamma_0<m^s_{k+1,r}<\gamma_1,\\ 1, & \gamma_1<m^s_{k+1,r}<\gamma_2,\\ \vdots & \vdots\\ L-1, & \gamma_{L-1}<m^s_{k+1,r}<\gamma_L,\end{cases} \qquad (11)
$$

where $m^s_{k+1,q}$ is the quantized measurement of the s^{th} node, and $\gamma_0,\gamma_1,\ldots,\gamma_L$ are the predetermined thresholds for a $K=\log_2 L$ bit quantizer, where L is the quantization level. The quantization thresholds are assumed to be identical at each node for simplicity. Given target state $\boldsymbol{x}_{k+1}$, the probability that $m^s_{k+1,q}$ takes value l is clearly as follows:

$$
\begin{aligned}
&p(m^s_{k+1,q}=l|\boldsymbol{x}_{k+1})\\
&=p(\gamma_l<m^s_{k+1,r}<\gamma_{l+1}|\boldsymbol{x}_{k+1})\\
&=Q\left(\frac{\gamma_l-h^s_{k+1}}{r_m}\right)-Q\left(\frac{\gamma_{l+1}-h^s_{k+1}}{r_m}\right)\\
&=Q\left(\frac{\gamma_l-h^s_{k+1}}{\sqrt{r^2+\left(\frac{\partial h^s_{k+1}}{\partial x^s_{k+1}}\right)^2 r_x^2+\left(\frac{\partial h^s_{k+1}}{\partial y^s_{k+1}}\right)^2 r_y^2}}\right) \qquad (12)\\
&\quad-Q\left(\frac{\gamma_{l+1}-h^s_{k+1}}{\sqrt{r^2+\left(\frac{\partial h^s_{k+1}}{\partial x^s_{k+1}}\right)^2 r_x^2+\left(\frac{\partial h^s_{k+1}}{\partial y^s_{k+1}}\right)^2 r_y^2}}\right),
\end{aligned}
$$

where $Q(\cdot)$ denotes the complementary distribution function of a standard Gaussian distribution with zero mean and unit variance:

$$
Q(x)=\int_x^\infty \frac{1}{\sqrt{2\pi}}\exp\left(-\frac{t^2}{2}\right)\mathrm{d}t. \qquad (13)
$$

3 Multi-sensor weighted particle filter with mutual information

In this section, MI between the underwater node's measurement and the target state is introduced for fusion weights. Then our MSWPF is designed to track the underwater target.

3.1 Mutual information between measurements and the target

In the view of information theory, measurements from sensor nodes contain information about the target. Entropy (specifically, Shannon entropy) is a fundamental notion in information theory (Shannon, 2001) and represents the amount of information held in a random variable. Moreover, MI quantifies the amount of information about one random variable provided by the other random variable, which is intricately linked to the entropy of the random variable. For the sensor management problem, an MI-based selection metric has been widely studied in Wang et al. (2005), Hoffmann and Tomlin (2010), and Masazade et al. (2010), in which sensors were selected to maximize the MI between nodes' measurements and the target state. Because MI can quantify the information about the target state provided by a node's measurement, it may have an effect on fusion weights of selected nodes. To design our MSWPF,

we calculate the MI between the underwater node's measurement and the target state.

According to the definition, MI between the measurement $m^s_{k+1,q}$ and target state $\boldsymbol{x}_{k+1}$ can be written as

$$\begin{aligned} I(\boldsymbol{x}_{k+1}, m^s_{k+1,q}) &= H(\boldsymbol{x}_{k+1}) - H(\boldsymbol{x}_{k+1}|m^s_{k,q}) \\ &= H(m^s_{k+1,q}) - H(m^s_{k+1,q}|\boldsymbol{x}_{k+1}), \end{aligned} \tag{14}$$

where $H(\cdot)$ means the function of entropy.

The entropy and conditional entropy of $m^s_{k+1,q}$ are defined as follows:

$$H(m^s_{k+1,q}) = -\sum_{m^s_{k+1,q}} p(m^s_{k+1,q}) \log p(m^s_{k+1,q}), \tag{15}$$

$$\begin{aligned} H(m^s_{k+1,q}|\boldsymbol{x}_{k+1}) = -\sum_{m^s_{k+1,q}} \int_{\boldsymbol{x}_{k+1}} \big\{ & p(m^s_{k+1,q}, \boldsymbol{x}_{k+1}) \\ & \cdot \log p(m^s_{k+1,q}|\boldsymbol{x}_{k+1}) \mathrm{d}\boldsymbol{x}_{k+1} \big\}, \end{aligned} \tag{16}$$

where $p(m^s_{k+1,q})$ can be calculated as

$$p(m^s_{k+1,q}) = \int_{\boldsymbol{x}_{k+1}} p(m^s_{k+1,q}|\boldsymbol{x}_{k+1}) p(\boldsymbol{x}_{k+1}) \mathrm{d}\boldsymbol{x}_{k+1}. \tag{17}$$

Because Eq. (17) has no closed-form solution to $p(m^s_{k+1,q})$, particle approximation is adopted to obtain the approximated result. In Eq. (18), we use predicted particles to approximate $p(m^s_{k+1,q})$:

$$\begin{aligned} p(m^s_{k+1,q}) &= \int_{\boldsymbol{x}_{k+1}} p(m^s_{k+1,q}|\boldsymbol{x}_{k+1}) p(\boldsymbol{x}_{k+1}) \mathrm{d}\boldsymbol{x}_{k+1} \\ &\approx \frac{1}{N} \sum_{i=1}^{N} p(m^s_{k+1,q}|\boldsymbol{x}^i_{k+1|k}), \end{aligned} \tag{18}$$

where $\boldsymbol{x}^i_{k+1|k}$ is the i^{th} predicted particle, and all predicted particles have an equal importance weight $1/N$. The predicted particles can be provided by the MSWPF, which will be introduced in the next subsection. Substituting Eq. (18) into Eq. (16), $H(m^s_{k+1,q})$ can be rewritten as

$$\begin{aligned} H(m^s_{k+1,q}) = -\sum_{l=0}^{L-1} \left\{ \frac{1}{N} \sum_{i=1}^{N} p(m^s_{k+1,q} = l|\boldsymbol{x}^i_{k+1|k}) \right\} \\ \cdot \log \left\{ \frac{1}{N} \sum_{i=1}^{N} p(m^s_{k+1,q} = l|\boldsymbol{x}^i_{k+1|k}) \right\}. \end{aligned} \tag{19}$$

Next, similar methods are adopted to calculate the conditional entropy $H(m^s_{k+1,q}|\boldsymbol{x}_{k+1})$. Note that the joint distribution can be expanded by using the chain rule:

$$p(m^s_{k+1,q}, \boldsymbol{x}_{k+1}) = p(m^s_{k+1,q}|\boldsymbol{x}_{k+1}) p(\boldsymbol{x}_{k+1}). \tag{20}$$

Substituting Eq. (20) into Eq. (16), we have

$$\begin{aligned} H(m^s_{k+1,q}|\boldsymbol{x}_{k+1}) = -\sum_{m^s_{k+1,q}} \int_{\boldsymbol{x}_{k+1}} \{ & p(m^s_{k+1,q}|\boldsymbol{x}_{k+1}) \\ & \cdot \log p(m^s_{k+1,q}|\boldsymbol{x}_{k+1}) p(\boldsymbol{x}_{k+1}) \mathrm{d}\boldsymbol{x}_{k+1} \}. \end{aligned} \tag{21}$$

Then we use the same particles to approximate $H(m^s_{k+1,q}|\boldsymbol{x}_{k+1})$ as

$$\begin{aligned} & H(m^s_{k+1,q}|\boldsymbol{x}_{k+1}) \\ & = -\sum_{l=0}^{L-1} \left\{ \frac{1}{N} \sum_{i=1}^{N} \{ p(m^s_{k+1,q} = l|\boldsymbol{x}^i_{k+1|k}) \right. \\ & \quad \left. \cdot \log p(m^s_{k+1,q} = l|\boldsymbol{x}^i_{k+1|k}) \} \right\}. \end{aligned} \tag{22}$$

Finally, by using Eqs. (19) and (22), the MI $I(\boldsymbol{x}_{k+1}, m^s_{k+1,q})$ in Eq. (14) is calculated as follows:

$$\begin{aligned} & I(\boldsymbol{x}_{k+1}, m^s_{k+1,q}) \\ & = -\sum_{l=0}^{L-1} \left\{ \frac{1}{N} \sum_{i=1}^{N} p(m^s_{k+1,q} = l|\boldsymbol{x}^i_{k+1|k}) \right\} \\ & \quad \cdot \log \left\{ \frac{1}{N} \sum_{i=1}^{N} p(m^s_{k+1,q} = l|\boldsymbol{x}^i_{k+1|k}) \right\} \\ & \quad + \sum_{l=0}^{L-1} \frac{1}{N} \sum_{i=1}^{N} p(m^s_{k+1,q} = l|\boldsymbol{x}^i_{k+1|k}) \\ & \quad \cdot \log p(m^s_{k+1,q} = l|\boldsymbol{x}^i_{k+1|k}). \end{aligned} \tag{23}$$

So far, we have obtained the MI for each underwater node's measurement and the target state. Note that the MI does not use measurements at time $k+1$; this means that if we have already known the estimated target state at time k, we can estimate the MI at time $k+1$. Because it is related to the information about the target state that is provided by measurement, the fusion center can use the MI to determine fusion weights of selected nodes and design the MSWPF. The results will be presented in the next subsection.

3.2 Multi-sensor weighted particle filter with mutual information

PF is an efficient way to solve nonlinear and non-Gaussian problems. Readers can refer to Gordon et al. (1993), Arulampalam et al. (2002), Ruan

et al. (2003), and Duan et al. (2008) for details. In our previous study, we designed a multi-sensor PF with quantized measurements to track underwater targets (Zhang Q et al., 2015; Liu et al., 2016). However, the problem of node fusion weights was not considered; we simply assumed that the information from all selected nodes was equal. In this subsection, we design a novel MSWPF to overcome this problem.

Assume that N_s sensor nodes take part in tracking the underwater target and provide the fusion center with their quantized measurements at each sampling interval. Once receiving measurements vector $\boldsymbol{m}_{k+1,q}=[m^1_{k+1,q},m^2_{k+1,q},\dots,m^{N_s}_{k+1,q}]^{\mathrm{T}}$, the fusion center merges measurements into a single multi-sensor measurement likelihood. For the traditional multi-sensor PF, the measurement likelihood over all N_s nodes is

$$p(\boldsymbol{m}_{k+1,q}|\boldsymbol{x}_{k+1})=\prod_{s=1}^{N_s}p(m^s_{k+1,q}|\boldsymbol{x}_{k+1}). \tag{24}$$

However, information from different nodes is not equal. It is crucial to merge measurements with different weights. Let $\boldsymbol{\alpha}_{k+1}=[\alpha^1_{k+1},\alpha^2_{k+1},\dots,\alpha^{N_s}_{k+1}]$ denote the weight vector of selected nodes. The joint measurement likelihood is the fusion of single likelihood over all N_s nodes; the weighted multi-sensor measurement likelihood is defined as

$$p(\boldsymbol{m}_{k+1,q}|\boldsymbol{x}_{k+1})=\prod_{s=1}^{N_s}\left(p(m^s_{k+1,q}|\boldsymbol{x}_{k+1})\right)^{\alpha^s_{k+1}}, \tag{25}$$

$$\sum_{s=1}^{N_s}\alpha^s_{k+1}=1. \tag{26}$$

As for the calculation of fusion weights, the MI between the measurement and the target state is used. According to the definition of MI, the larger the MI is, the larger the weight of the node should be. Thus, fusion weights of selected nodes are

$$\alpha^s_{k+1}=\frac{I^s_{k+1}}{\sum_{j=1}^{N_s}I^j_{k+1}},\ s=1,2,\dots,N_s, \tag{27}$$

where I^s_{k+1} denotes the MI between measurement $m^s_{k+1,q}$ and target state $\boldsymbol{x}_{k+1}$, and it can be calculated by Eq. (23). Substituting Eqs. (12) and (27) into Eq. (25), we obtain the weighted multi-sensor measurement likelihood.

Fig. 2 shows the main idea of weighted fusion. Each selected node sends both its quantized measurement m^s_{k+1} and predicted MI I^s_{k+1} to the fusion center. Then the fusion center determines weights by Eq. (27) and calculates the weighted multi-sensor measurement likelihood by Eq. (25).

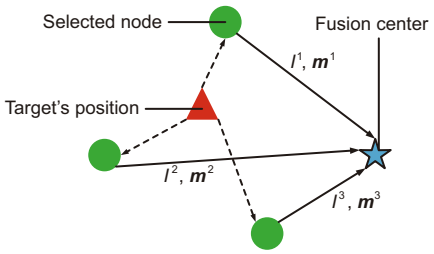

Fig. 2 Weighted fusion

If adopting the transition prior $p(\boldsymbol{x}_{k+1}|\boldsymbol{x}_k)$ as the proposal distribution (Arulampalam et al., 2002), the importance weight of the i^{th} particle $\boldsymbol{x}^i_{k+1}$ can be calculated as

$$w^i_{k+1}=w^i_k\ p(\boldsymbol{m}_{k+1,q}|\boldsymbol{x}^i_{k+1}). \tag{28}$$

Algorithm 1 summarizes the above MSWPF with N particles.

4 Node selection based on posterior Cramer-Rao lower bound (PCRLB)

In this section, the relationship between PCRLB and target-node geometry is introduced as the metric of node selection. Then a selection scheme is presented based on PCRLB.

4.1 Relationship between PCRLB and target-node geometry

PCRLB provides the theoretical performance limit for a Bayesian estimator (Tichavsky et al., 1998; Taylor et al., 2003; Zhang et al., 2005; Ozdemir et al., 2009; Masazade et al., 2012). Let $p(\boldsymbol{m}_{k+1,q},\boldsymbol{x}_{k+1})$ be the joint probability density of the quantized measurements $\boldsymbol{m}_{k+1,q}$ and unknown state $\boldsymbol{x}_{k+1}$, and $\hat{\boldsymbol{x}}_{k+1}$ be an estimate of $\boldsymbol{x}_{k+1}$. PCRLB on the mean squared estimation error has the following form:

$$E[\hat{\boldsymbol{x}}_{k+1}-\boldsymbol{x}_{k+1}][\hat{\boldsymbol{x}}_{k+1}-\boldsymbol{x}_{k+1}]^{\mathrm{T}}\geq\boldsymbol{J}^{-1}_{k+1}, \tag{29}$$

where $\boldsymbol{J}_{k+1}\in\mathbb{R}^{4\times4}$ is a Fisher information matrix (FIM) with the element

$$\boldsymbol{J}_{k+1}(i,j)=E_{p(\boldsymbol{m}_{k+1,q},\boldsymbol{x}_{k+1})}\left[-\frac{\partial^2\log p(\boldsymbol{m}_{k+1,q},\boldsymbol{x}_{k+1})}{\partial\boldsymbol{x}_{k+1}(i)\partial\boldsymbol{x}_{k+1}(j)}\right], \tag{30}$$

Algorithm 1 Multi-sensor weighted particle filter with mutual information

if $k=0$ **then**
  // Particle initialization:
  for $i=1,2,\ldots,N$ **do**
    Draw particle $\boldsymbol{x}_k^i$ from the prior target state $p(\boldsymbol{x}_0)$
  end for
end if
for $k=1,2,\ldots$ **do**
  // Importance sampling:
  for $i=1,2,\ldots,N$ **do**
    Sample $\boldsymbol{x}_{k+1}^i \sim p(\boldsymbol{x}_{k+1}|\boldsymbol{x}_k^i)$
  end for
  for $s=1,2,\ldots,N_s$ **do**
    Update the fusion weight vector $\boldsymbol{\alpha}_k$ by Eqs. (10), (19), and (26)
  end for
  for $i=1,2,\ldots,N$ **do**
    Update the importance weights by Eqs. (10), (24), and (27)
  end for
  for $i=1,2,\ldots,N$ **do**
    Normalize the importance weights $\tilde{w}_{k+1}^i = w_{k+1}^i / \left(\sum_{j=1}^N w_{k+1}^j\right)$
  end for
  // Resampling:
  for $i=1,2,\ldots,N$ **do**
    Multiply (Suppress) $\boldsymbol{x}_{k+1}^i$ with high (low) weights $\tilde{w}_{k+1}^i$ to obtain N particles
    Set $w_{k+1}^i = \tilde{w}_{k+1}^i = 1/N$
  end for
  // Estimate the state and covariance:
  $\hat{\boldsymbol{x}}_{k+1} = \sum_{i=1}^N \left(w_{k+1}^i \boldsymbol{x}_{k+1}^i\right)$,
  $\boldsymbol{P}_{k+1} = \sum_{i=1}^N w_{k+1}^i \left(\boldsymbol{x}_{k+1}^i - \hat{\boldsymbol{x}}_{k+1}\right)\left(\boldsymbol{x}_{k+1}^i - \hat{\boldsymbol{x}}_{k+1}\right)^{\mathrm{T}}$
end for

where $\boldsymbol{J}_{k+1}(i,j)$ denotes the i^{th} row and j^{th} column element of $\boldsymbol{J}_{k+1}$, $E_{p(\boldsymbol{m}_{k+1,q},\boldsymbol{x}_{k+1})}$ denotes the expectation with respect to $p(\boldsymbol{m}_{k+1,q},\boldsymbol{x}_{k+1})$, and $\boldsymbol{x}_{k+1}(i)$ denotes the i^{th} element of vector $\boldsymbol{x}_{k+1}$. Let $\nabla_{\boldsymbol{x}_{k+1}}^{\boldsymbol{x}_{k+1}} = \nabla_{\boldsymbol{x}_{k+1}} \nabla_{\boldsymbol{x}_{k+1}}^{\mathrm{T}}$ be the second-order partial derivative operator with respect to $\boldsymbol{x}_{k+1}$. Then Eq. (30) can be rewritten as

$$\boldsymbol{J}_{k+1} = E_{p(\boldsymbol{m}_{k+1,q},\boldsymbol{x}_{k+1})}\left[-\nabla_{\boldsymbol{x}_{k+1}}^{\boldsymbol{x}_{k+1}} \log p(\boldsymbol{m}_{k+1,q},\boldsymbol{x}_{k+1})\right]. \tag{31}$$

Due to $p(\boldsymbol{m}_{k+1,q},\boldsymbol{x}_{k+1}) = p(\boldsymbol{m}_{k+1,q}|\boldsymbol{x}_{k+1})p(\boldsymbol{x}_{k+1})$, $\boldsymbol{J}_{k+1}$ can be decomposed into two parts:

$$\boldsymbol{J}_{k+1} = \boldsymbol{J}_{k+1}^{\mathrm{D}} + \boldsymbol{J}_{k+1}^{\mathrm{P}}, \tag{32}$$

where

$$\begin{aligned} \boldsymbol{J}_{k+1}^{\mathrm{D}} &= E_\theta\left[-\nabla_{\boldsymbol{x}_{k+1}}^{\boldsymbol{x}_{k+1}} \log p(\boldsymbol{m}_{k+1,q}|\boldsymbol{x}_{k+1})\right], \\ \theta &= p(\boldsymbol{m}_{k+1,q}|\boldsymbol{x}_{k+1})p(\boldsymbol{x}_{k+1}), \end{aligned} \tag{33}$$

$$\boldsymbol{J}_{k+1}^{\mathrm{P}} = E_{p(\boldsymbol{x}_{k+1})}\left[-\nabla_{\boldsymbol{x}_{k+1}}^{\boldsymbol{x}_{k+1}} \log p(\boldsymbol{x}_{k+1})\right]. \tag{34}$$

Note that $\boldsymbol{J}_{k+1}^{\mathrm{D}}$ represents the Fisher information obtained from the quantized measurements and $\boldsymbol{J}_{k+1}^{\mathrm{P}}$ represents prior Fisher information. In our previous study, we proved that PCRLB depends on the target-node geometry. Hence, PCRLB can be used to select the best N_s nodes to take part in the tracking task. Specifically, the nodes that minimize PCRLB will be selected. The derivations of $\boldsymbol{J}_{k+1}^{\mathrm{D}}$ and $\boldsymbol{J}_{k+1}^{\mathrm{P}}$ are not given here; readers can refer to Liu et al. (2016) and Zhang et al. (2016) for details.

4.2 Local node selection scheme

Having derived the relationship between PCRLB and target-node geometry, we present how to select the best N_s nodes to track an underwater target.

We define nodes that may have an opportunity to take part in the tracking task at each interval as qualified candidates, and the best N_s nodes are selected from these qualified candidates. Fig. 3 shows the main idea in selecting qualified candidates. The target position at time $k+1$ can be predicted by state model (1), and then distance d_{k+1}^{sp} between the s^{th} node and the predicted target position can be calculated. Then it can be used to select qualified candidates. Obviously, qualified candidates should satisfy the following constraint:

$$d_{k+1}^{\mathrm{sp}} \le r, \tag{35}$$

where r denotes the node's sensing range.

To select the best N_s nodes from qualified candidates, we define the Boolean variable $g_s \in \{0,1\}$,

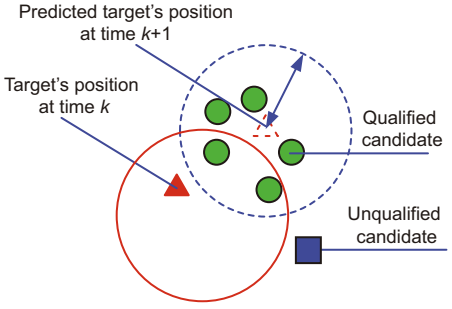

Fig. 3 Selection of qualified candidates

where $s = 1, 2, \ldots, N_q$, and N_q stands for the number of qualified candidates. Thus, the node selection problem can be formulated as

$$\begin{aligned} \min_{\boldsymbol{g}_{k+1}} \quad & -\det(\boldsymbol{J}_{k+1}(\boldsymbol{g}_{k+1})) \\ \text{s.t.} \quad & \sum_{s=1}^{N_q} g_s = N_s,\ g_s \in \{0,1\}, \\ & s = 1, 2, \ldots, N_q, \end{aligned} \tag{36}$$

where $\boldsymbol{g}_{k+1} = [g_1, g_2, \ldots, g_{N_q}]^{\mathrm{T}}$ stands for the node selection scheme at time $k+1$, $g_s = 1$ means node s is selected, and $g_s = 0$ means node s is not selected.

5 Simulation

We present the simulation results of underwater target tracking by our scheme. Our scheme is based on MSWPF, in which fusion weights are determined by MI, and our scheme is called good weight (GW). Two different schemes are also simulated for comparison. One is the equal weight (EW) scheme; the fusion weights are not considered in this scheme, which means all nodes have an equal weight. The other is the bad weight (BW) scheme. In this scheme, we determine fusion weights inverse to MI; then the node with the most information receives the minimum weight, and a bad tracking performance is obtained. To verify our scheme, simulations are performed in 2D and 3D scenarios. In the 2D scenario, sensor nodes are deployed at a fixed depth and the target is moving in a plane at a known depth. In the 3D scenario, sensor nodes are deployed throughout the monitoring area and the target is moving in the 3D space.

5.1 Results of 2D scenario

1. Simulation setup

Sensor nodes are uniformly deployed over a 1000 m × 1000 m region; the target is moving in the plane at depth $h = 50$ m and the distance between adjacent nodes is $d = 120$ m (Fig. 4); the sensing range of a node is $r_{\mathrm{s}} = 160$ m; the target's source-level sound pressure is $S = 5 \times 10^4$; the number of selected nodes at each interval is $N_s = 3$; the actual initial state of the target is $\boldsymbol{x}_0 = [0,\ 10,\ 0,\ 10]^{\mathrm{T}}$; the initial estimate of the target is $\hat{\boldsymbol{x}}_0 = [5,\ 10,\ 5,\ 10]^{\mathrm{T}}$; the initial covariance matrix is $\boldsymbol{P}_0 = 10\,\boldsymbol{I}_{4\times4}$, where $\boldsymbol{I}$ is an identity matrix; the standard deviation of the measurement noise is assumed to be constant as $r = 5$; the standard deviation of the node's location noise is $r_x = r_y \in \{0, 2, 4, 6\}$; the standard deviation of the process noise is $q = 1$; the quantization level is $L \in \{2, 4, 6, 8\}$; the sampling interval is $T = 1$ s; the particle number is $N = 1000$; the Monte Carlo (MC) simulation runs MC = 100.

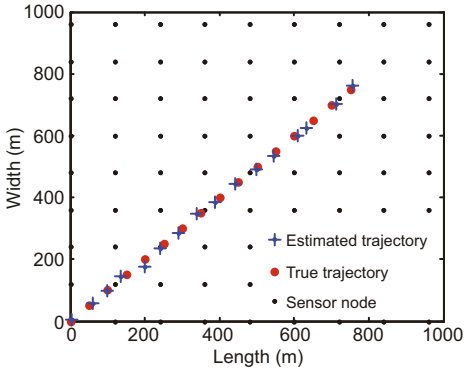

Fig. 4 2D simulation scenario

To indicate the accuracy of target tracking, we adopt the root-mean-square error (RMSE) to measure the tracking performance as

$$\varepsilon(k) = \sqrt{\sum_{i=1}^{\mathrm{MC}} \left(\frac{\left(\boldsymbol{x}_k^{i,1} - \hat{\boldsymbol{x}}_k^{i,1}\right)^2 + \left(\boldsymbol{x}_k^{i,3} - \hat{\boldsymbol{x}}_k^{i,3}\right)^2}{\mathrm{MC}} \right)}, \tag{37}$$

where $\left(\boldsymbol{x}_k^{i,1}, \boldsymbol{x}_k^{i,3}\right)$ and $\left(\hat{\boldsymbol{x}}_k^{i,1}, \hat{\boldsymbol{x}}_k^{i,3}\right)$ are the true and estimated locations of the target at time k in the i^{th} simulation, respectively.

2. Comparison of results

Simulation results of the GW, EW, and BW schemes with $L = \{4, 6, 8\}$ are shown in Figs. 5–7. We can see that the GW scheme achieves the best tracking performance. This is because the GW scheme determines fusion weights by MI, and the node with the larger MI can provide more useful information about the target. Because the BW scheme determines fusion weights inverse to the MI, the node with more useful information has a smaller weight, leading to the worst performance. For the EW scheme, all selected nodes have an equal weight and hence its performance is between those of the other two schemes.

Fig. 8 shows the corresponding average tracking errors of the GW, EW, and BW schemes with $L = \{2, 4, 6, 8\}$. It is obvious that the tracking error decreases with an increase of quantization level L, since the loss of measurement decreases with an

increase of quantization level L. Table 1 shows the average simulation error and the improvement using the GW compared to the EW scheme. Interestingly, the GW scheme performs much better than the EW scheme with an increase of the quantization level L. This is because as L increases, the estimated MI between the measurement and target is more precise, which results in better fusion weights. Hence, the GW scheme has better tracking performance with an increase of the quantization level L. Note that if L is large enough, the improvement in the GW scheme may decrease because measurements have provided too much information. However, large L means heavy energy consumption and computation burden, which is not practical for UWSNs.

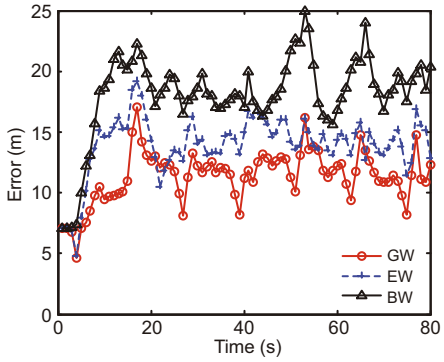

Fig. 5 2D scenario: tracking errors for the GW, EW, and BW schemes with $L = 4$ (over 100 MC runs)

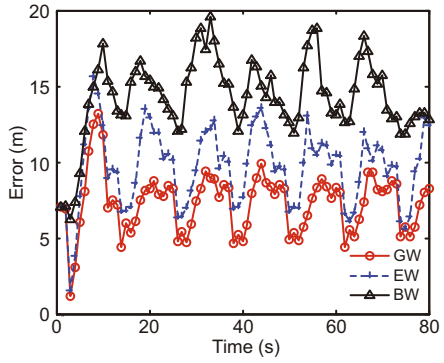

Fig. 6 2D scenario: tracking errors for the GW, EW, and BW schemes with $L = 6$ (over 100 MC runs)

Table 1 2D scenario: average tracking errors with different quantization level L

L	Average tracking error (m)			Improvement
	GW	EW	BW	
2	27.050	31.800	31.92	14.9%
4	11.380	13.950	18.14	18.4%
6	7.312	9.694	14.30	24.6%
8	6.265	8.581	13.15	27.0%

Simulation results of the GW, EW, and BW schemes with $r_x = r_y \in \{2, 4, 6\}$ are plotted in Figs. 9–11. It is not surprising that the GW scheme has the best performance and BW has the worst one. As shown in Table 2 and Fig. 12, with an increase in the node's location noise, the performance of the GW scheme is gradually degraded to that of the EW scheme, because of the effect of the node's location uncertainty. With an increase in the node's location noise, the estimate of MI is not quite precise, which means that the values of fusion weights are not good enough, leading to a decreased improvement. The results show that the uncertainty of the node's location is still an important problem for the underwater

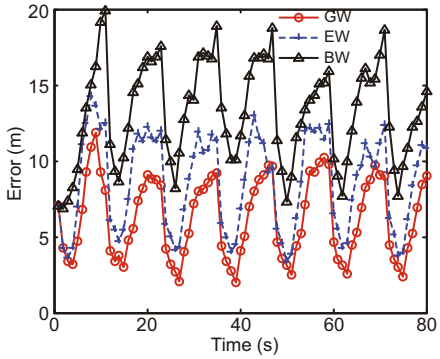

Fig. 7 2D scenario: tracking errors for the GW, EW, and BW schemes with $L = 8$ (over 100 MC runs)

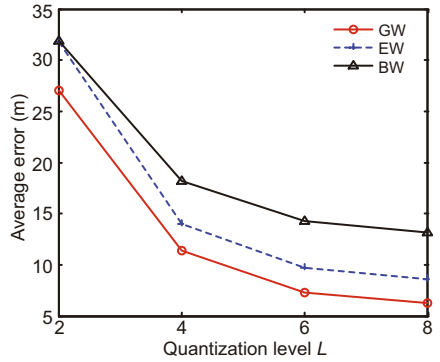

Fig. 8 2D scenario: average tracking errors for the GW, EW, and BW schemes with different L (over 100 MC runs)

Table 2 2D scenario: average tracking errors with different node location noise r_x and r_y

r_x, r_y	Average tracking error (m)			Improvement
	GW	EW	BW	
0	6.265	8.581	13.15	27.0%
2	7.162	9.074	15.01	21.1%
4	8.611	10.330	16.37	16.6%
6	11.040	12.280	18.46	10.1%

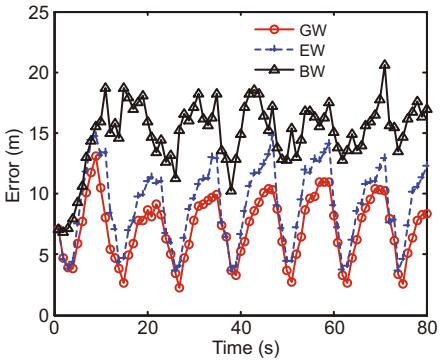

Fig. 9 2D scenario: tracking errors for the GW, EW, and BW schemes with $r_x = r_y = 2$ (over 100 MC runs)

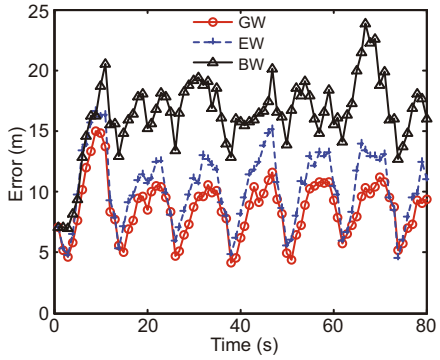

Fig. 10 2D scenario: tracking errors for the GW, EW, and BW schemes with $r_x = r_y = 4$ (over 100 MC runs)

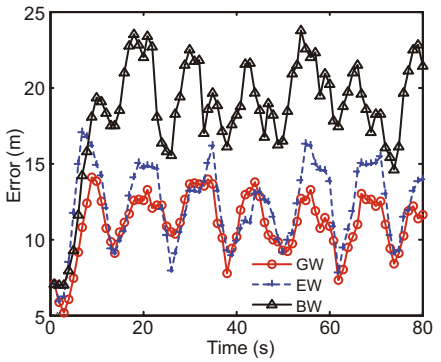

Fig. 11 2D scenario: tracking errors for the GW, EW, and BW schemes with $r_x = r_y = 6$ (over 100 MC runs)

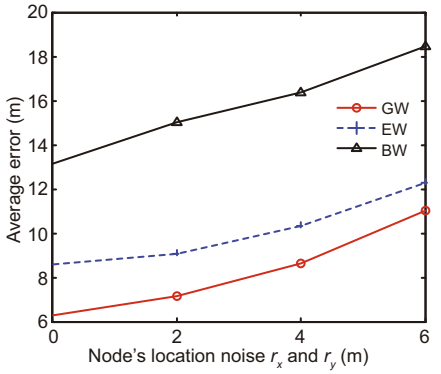

Fig. 12 2D scenario: average tracking errors for the GW, EW, and BW schemes with different r_x and r_y

environment; it has a great effect not only on fusion weights, but also on tracking performance. We will consider a better solution to node location uncertainty in our future work.

It is very interesting that tracking errors change periodically over time, mainly because of the regular node deployment (Fig. 4). In this regular network, the target will periodically return to the same place that it occupied previously, and tracking errors therefore change periodically over time. A similar phenomenon can be found in 3D results.

5.2 Results of the 3D scenario

In this subsection, a 3D example is simulated to verify the effectiveness of our scheme. Suppose the target model is a 3D CV model:

$$\boldsymbol{x}_{k+1} = \boldsymbol{F}_k \boldsymbol{x}_k + \boldsymbol{w}_k, \tag{38}$$

where the target state at time k is given by $\boldsymbol{x}_k = [x, v_x, y, v_y, z, v_z]^{\mathrm{T}}$, (x, y, z) is the target's position, v_x, v_y, and v_z are the target velocities in x, y, and z coordinates, respectively, $\boldsymbol{F}_k$ is the state transition matrix, and the process noise $\boldsymbol{w}_k$ is assumed to be Gaussian with zero mean and covariance matrix $\boldsymbol{Q}_k$. The state transition matrix and process noise covariance matrix are given as follows:

$$\boldsymbol{F}_k = \begin{bmatrix} 1 & T & 0 & 0 & 0 & 0 \\ 0 & 1 & 0 & 0 & 0 & 0 \\ 0 & 0 & 1 & T & 0 & 0 \\ 0 & 0 & 0 & 1 & 0 & 0 \\ 0 & 0 & 0 & 0 & 1 & T \\ 0 & 0 & 0 & 0 & 0 & 1 \end{bmatrix}, \tag{39}$$

$$\boldsymbol{Q}_k = q^2 \begin{bmatrix} \frac{T^3}{3} & \frac{T^2}{2} & 0 & 0 & 0 & 0 \\ \frac{T^2}{2} & T & 0 & 0 & 0 & 0 \\ 0 & 0 & \frac{T^3}{3} & \frac{T^2}{2} & 0 & 0 \\ 0 & 0 & \frac{T^2}{2} & T & 0 & 0 \\ 0 & 0 & 0 & 0 & \frac{T^3}{3} & \frac{T^2}{2} \\ 0 & 0 & 0 & 0 & \frac{T^2}{2} & T \end{bmatrix}, \tag{40}$$

where T is the sampling interval.

1. Simulation setup

Sensor nodes are uniformly deployed over a 400 m × 400 m × 400 m region; the target is moving in the 3D space according to the motion model given by

Eqs. (36)–(38); the distance between adjacent nodes is $d = 80$ m (Fig. 13); the sensing range of a node is $r_s = 120$ m; the target's source-level sound pressure is $S = 5 \times 10^4$; the number of selected nodes at each interval is $N_s = \{3, 4, 5\}$; the actual initial state of the target is $\boldsymbol{x}_0 = [0,\ 5,\ 0,\ 5,\ 0,\ 5]^{\mathrm{T}}$; the initial estimate of the target is $\hat{\boldsymbol{x}}_0 = [5,\ 5,\ 5,\ 5,\ 5,\ 5]^{\mathrm{T}}$; the initial covariance matrix is $\boldsymbol{P}_0 = 10\,\boldsymbol{I}_{6\times 6}$; the standard deviation of the measurement noise is assumed to be constant at $r = 5$; the standard deviation of the node's location noise is $r_x = r_y = 2$; the standard deviation of the process noise is $q = 1$; the quantization level is $L \in \{2, 4, 6, 8\}$; the sampling interval is $T = 1$ s; the particle number is $N = 1000$; the Monte Carlo simulation runs MC = 100.

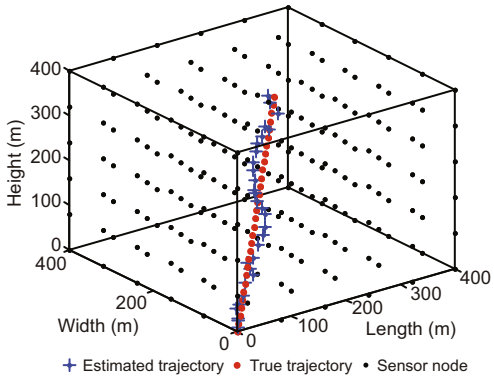

Fig. 13 3D simulation scenario

2. Comparison of results

Simulation results of different numbers of selected nodes $N_s = \{3, 4, 5\}$ are plotted in Fig. 14, and the corresponding average tracking errors are shown in Table 3. The tracking error decreases with an increase in the number of nodes. This can be explained as follows: the more nodes that are selected to take part in tracking, the more information the fusion center will obtain. Table 3 shows that the improvement, compared to the EW scheme, decreases with an increase in the number of nodes, because the fusion center can obtain enough information about the target with a large number of nodes ($N_s = 5$), which may offset the loss caused by equal weights.

The results of the GW scheme with three nodes (GW-3), EW with three nodes (EW-3), and EW with five nodes (EW-5) are plotted in Fig. 15. Like the results in the 2D scenario, with an equal number of selected nodes ($N_s = 3$), GW-3 has an obvious improvement on tracking performance compared to

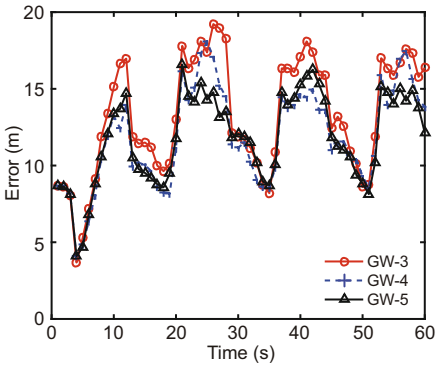

Fig. 14 3D scenario: tracking errors for the GW scheme with different selected node number N_s (over 100 MC runs)

Table 3 3D scenario: average tracking errors with different numbers of selected nodes (N_s)

N_s	Average tracking error (m)		Improvement
	GW	EW	
3	13.26	17.20	22.9%
4	11.92	15.17	21.4%
5	11.81	14.00	15.7%

EW-3. The EW-5 error is approximately equal to the GW-3 one. However, it will cause more energy consumption because it selects more nodes. In addition, an exhaustive search is required to select the best N_s nodes; if N_s is a large number, the exhaustive search is not computationally efficient. The average computation time of a sampling interval and average time of one MC simulation are shown in Figs. 16 and 17 and Table 4. The results show that EW-3 performs a little more efficiently than GW-3, because it does not need to calculate MI or fusion weights, but it has the worst performance. As for GW-3 and EW-5, the former scheme performs not only more efficiently but also more precisely. Hence, our scheme is a precise and energy-efficient solution for target tracking in UWSNs.

Table 4 3D scenario: average time of one MC with different quantization level L

L	Average time of one MC (s)		
	GW-3	EW-3	EW-5
2	6.778	6.566	7.869
4	10.140	9.314	11.320
6	11.670	10.520	11.870
8	13.180	12.710	15.490

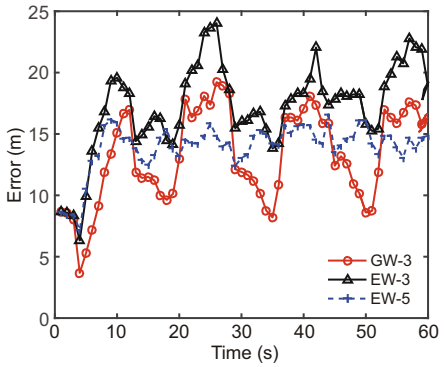

Fig. 15 3D scenario: tracking errors for GW-3, EW-3, and EW-5 (over 100 MC runs)

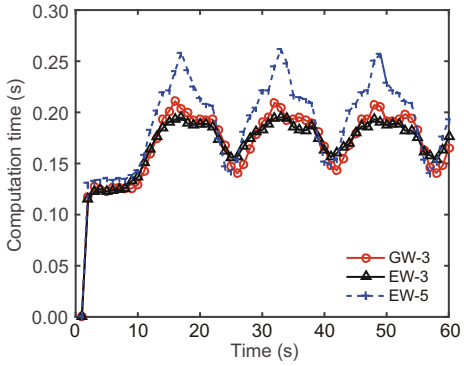

Fig. 16 3D scenario: average computation time for GW-3, EW-3, and EW-5 (over 100 MC runs)

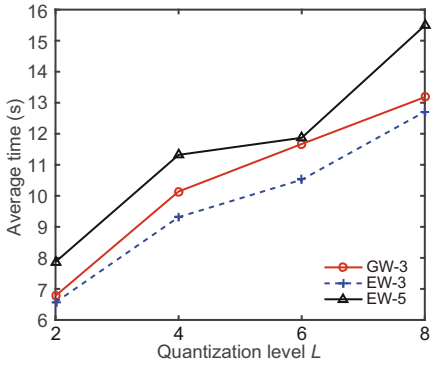

Fig. 17 3D scenario: average time of one MC for GW-3, EW-3, and EW-5 with different quantization level L (over 100 MC runs)

6 Conclusions and future work

We have studied a weighted fusion scheme for target tracking in UWSNs. We have presented a novel multi-sensor weighted particle filter (MSWPF) and a corresponding tracking scheme. To find a proper solution to determine fusion weights, the mutual information (MI) between a node's measurement and the target state was calculated. To verify the effectiveness of our scheme, 2D and 3D simulation scenarios have been carried out. The results showed that with fusion weights determined by MI, our scheme achieved better tracking performance than existing schemes.

However, there are many problems for target tracking in a real sea environment, such as clock synchronization and channel fading. Further work will focus on these problems and extend the algorithms to multiple target-tracking problems to develop an experimental platform in a real sea environment.

References

Arulampalam M, Maskell S, Gordon N, et al., 2002. A tutorial on particle filters for online nonlinear/non-Gaussian Bayesian tracking. *IEEE Trans Signal Process*, 50(2):174-188. https://doi.org/10.1109/78.978374

Asif M, Rizal M, Yahya A, 2006. An active contour for underwater target tracking and navigation. Int Conf on Man-Machine Systems, p.1-6.

Baumgartner K, Ferrari S, Rao A, 2009a. Optimal control of an underwater sensor network for cooperative target tracking. *IEEE J Ocean Eng*, 34(4):678-697. https://doi.org/10.1109/JOE.2009.2025643

Baumgartner K, Ferrari S, Wettergren T, 2009b. Robust deployment of dynamic sensor networks for cooperative track detection. *IEEE Sens J*, 9(9):1029-1048. https://doi.org/10.1109/JSEN.2009.2025836

Chen Y, Pan Q, Liang Y, et al., 2010. AWCL: adaptive weighted centroid target localization algorithm based on RSSI in WSN. IEEE Int Conf on Computer Science and Information Technology, p.331-336. https://doi.org/10.1109/ICCSIT.2010.5565022

Dalberg E, Lauberts A, Lennartsson R, et al., 2006. Underwater target tracking by means of acoustic and electromagnetic data fusion. 9th Int Conf on Information Fusion, p.1-7. https://doi.org/10.1109/ICIF.2006.301613

Doug H, Bruce D, Shozo M, 2002. Autonomous distributed systems: multiple-level distributed data fusion for future DADS using Bayesian network technology. Technical Report, IET-TR-ADS-04. Information Extraction and Transport Inc., VA, USA.

Duan Z, Jilkov V, Li R, 2008. State estimation with quantized measurements: approximate MMSE approach. 11th Int Conf on Information Fusion, p.1-6. https://doi.org/10.1109/ICIF.2008.4632328

Georgy J, Noureldin A, Mellema G, 2012. Clustered mixture particle filter for underwater multitarget tracking in multistatic active sonobuoy systems. *IEEE Trans Syst Man Cybern Part C Appl Rev*, 42(4):547-560. https://doi.org/10.1109/TSMCC.2011.2154329

Gordon N, Salmond D, Smith A, 1993. Novel approach to nonlinear and non-Gaussian Bayesian state estimation. *IEE Proc F - Radar Signal Process*, 140(2):107-113. https://doi.org/10.1049/ip-f-2.1993.0015

Han G, Jiang J, Shu L, et al., 2012. Localization algorithms of underwater wireless sensor networks: a survey. *Sensors*, 12(2):2026-2061. https://doi.org/10.3390/s120202026

Hoffmann G, Tomlin C, 2010. Mobile sensor network control using mutual information methods and particle filters. *IEEE Trans Autom Contr*, 55(1):32-47. https://doi.org/10.1109/TAC.2009.2034206

Huang Y, Liang W, Yu H, et al., 2008. Target tracking based on a distributed particle filter in underwater sensor networks. *Wirel Commun Mob Comput*, 8(8):1023-1033. https://doi.org/10.1002/wcm.660

Isbitiren G, Akan O, 2011. Three-dimensional underwater target tracking with acoustic sensor networks. *IEEE Trans Veh Tech*, 60(8):3897-3906. https://doi.org/10.1109/TVT.2011.2163538

Javadi S, Peiravi A, 2015. Fusion of weighted decisions in wireless sensor networks. *IET Wirel Sens Syst*, 5(2):97-105. https://doi.org/10.1049/iet-wss.2013.0116

Liang Q, Cheng X, 2009. Underwater acoustic sensor networks: target size detection and performance analysis. *Ad Hoc Netw*, 7(4):803-808. https://doi.org/10.1109/ICC.2008.593

Liu M, Zhang Q, Zhang S, 2016. Computationally efficient target-node geometry selection for target tracking in UWSNs. 19th Int Conf on Information Fusion, p.1608-1615.

Masazade E, Niu R, Varshney P, et al., 2010. Energy aware iterative source localization for wireless sensor networks. *IEEE Trans Signal Process*, 58(9):4824-4835. https://doi.org/10.1109/TSP.2010.2051433

Masazade E, Niu R, Varshney P, 2012. Dynamic bit allocation for object tracking in wireless sensor networks. *IEEE Trans Signal Process*, 60(10):5048-5063. https://doi.org/10.1109/TSP.2012.2204257

Ozdemir O, Niu R, Varshney P, 2009. Channel aware target localization with quantized data in wireless sensor networks. *IEEE Trans Signal Process*, 57(3):1190-1202. https://doi.org/10.1109/TSP.2008.2009893

Pettersson M, Zetterberg V, Claesson I, 2005. Detection and imaging of moving targets in wideband SAS using fast time backprojection combined with space-time processing. MTS/IEEE Oceans, p.2388-2393. https://doi.org/10.1109/OCEANS.2005.1640123

Punithakumar K, Kirubarajan T, Hernandez M, 2006. Multisensor deployment using PCRLBs, incorporating sensor deployment and motion uncertainties. *IEEE Trans Aerosp Electr Syst*, 42(4):1474-1485. https://doi.org/10.1109/TAES.2006.314587

Ruan Y, Willett P, Marrs A, 2003. Fusion of quantized measurements via particle filtering. IEEE Aerospace Conf, p.1967-1978. https://doi.org/10.1109/AERO.2003.1235125

Shannon CE, 2001. A mathematical theory of communication. *ACM SIGMOBILE Mob Comput Commun Rev*, 5(1):3-55. https://doi.org/10.1145/584091.584093

Taylor R, Flanagan B, Uber J, 2003. Computing the recursive posterior Cramer-Rao bound for a nonlinear nonstationary system. IEEE Int Conf on Acoustics, Speech, and Signal Processing, p.673-676. https://doi.org/10.1109/ICASSP.2003.1201771

Tichavsky P, Muravchik C, Nehorai A, 1998. Posterior Cramer-Rao bounds for discrete-time nonlinear filtering. *IEEE Trans Signal Process*, 46(5):1386-1396. https://doi.org/10.1109/78.668800

Wang H, Yao K, Estrin D, 2005. Information-theoretic approaches for sensor selection and placement in sensor networks for target localization and tracking. *J Commun Netw*, 7(4):438-449. https://doi.org/10.1109/JCN.2005.6387986

Wang X, Xu M, Wang H, et al., 2012. Combination of interacting multiple models with the particle filter for three-dimensional target tracking in underwater wireless sensor networks. *Math Prob Eng*, 2012:1-16. https://doi.org/10.1155/2012/829451

Yu C, Lee K, Choi J, et al., 2008. Distributed single target tracking in underwater wireless sensor networks. SICE Annual Conf, p.1351-1356. https://doi.org/10.1109/SICE.2008.4654868

Zhang D, Liu M, Zhang S, 2016. Node selection for target tracking in UWSNs under measurement origin uncertainty. 35th Chinese Control Conf, p.5154-5159. https://doi.org/10.1109/ChiCC.2016.7554154

Zhang Q, Zhang S, Liu M, 2013. A clock synchronization independent localization scheme for underwater wireless sensor networks. 8th ACM Int Conf on Underwater Networks and Systems, p.152-156. https://doi.org/10.1145/2532378.2532386

Zhang Q, Liu M, Zhang S, et al., 2014. Node topology effect on target tracking based on underwater wireless sensor networks. 17th Int Conf on Information Fusion, p.1-8.

Zhang Q, Liu M, Zhang S, 2015. Node topology effect on target tracking based on UWSNs using quantized measurements. *IEEE Trans Cybern*, 45(10):2323-2335. https://doi.org/10.1109/TCYB.2014.2371232

Zhang S, Zhang Q, Liu M, 2014. A top-down positioning scheme for underwater wireless sensor networks. *Sci China Inform Sci*, 57(3):1-10. https://doi.org/10.1007/s11432-013-4797-6

Zhang X, Willett P, Bar-Shalom Y, 2005. Dynamic Cramer-Rao bound for target tracking in clutter. *IEEE Trans Aerosp Electr Syst*, 41(4):1154-1167. https://doi.org/10.1109/TAES.2005.1561880

Zhou S, Willett P, 2007. Submarine location estimation via a network of detection-only sensors. *IEEE Trans Signal Process*, 55(6):3104-3115. https://doi.org/10.1109/TSP.2007.893970